Acta Crystallographica Section A
Foundations of Crystallography
ISSN 0108-7673

Received 23 November 1999
Accepted 21 February 2000

X-ray dynamical diffraction: the concept of a locally plane wave

V. Mocella,[a]* Y. Epelboin[b] and J. P. Guigay[a]

[a]ESRF, European Synchrotron Radiation Facility, BP 220, 38043 Grenoble CEDEX, France, and [b]LMCP, UMR 7590 CNRS, Universités P. M. Curie et D. Diderot, Case 115, 75252 Paris CEDEX 05, France. Correspondence e-mail: mocella@esrf.fr

The long distance between the source and the experiment and the small source size, now available at third-generation synchrotron sources, leads to new optical characteristics for X-ray diffraction. It is shown that, under certain conditions, the intensity received by a point located on the exit surface of a crystal is described by the diffraction of a locally plane wave. Each point along the surface is influenced by a plane wave with a varying departure from Bragg angle. In such a case, it is possible to visualize the rocking curve of the crystal as a function of the position along the exit surface. This represents a topographic method to obtain the reflectivity curve of the crystal instead of the usual goniometric method. Applications will be described in a forthcoming paper.

1. Introduction

The usual formulations of X-ray dynamical diffraction consider two cases: either a point source located at infinity (plane wave) or a point source situated exactly on the entrance surface (Kato's spherical wave) (Kato, 1960, 1961*a*,*b*). Afanas'ev & Kohn (1977) have analyzed the case of a spherical wave impinging from a point source situated at an arbitrary distance from the crystal. Their work pointed out that the shape of the *Pendellösung* fringes is sensitive to the thickness of the crystal. These fringes differ from Kato's fringes (Kato & Lang, 1959) in the case of a thin crystal and the authors call them *anomalous Pendellösung fringes* (Aristov *et al.*, 1980). The authors did not investigate the effect of the coherence properties of the source: they used laboratory sources, without special arrangements.

To properly treat new-generation synchrotron sources, we have to take the coherence properties of the source into account. A first attempt has been made by Carvalho & Epelboin (1990), limiting their analysis to the case of an incident white beam.

In the present work, we consider a source located at a large distance L_0 from the crystal and discuss how the diffraction profile is affected by the source size (spatial coherence) and by the wavelength bandwidth (temporal coherence). We will explain why the crystal locally 'sees' a plane wave and how the intensity profile reproduces the reflectivity curve of the crystal (rocking curve) with a local correspondence between position and angular deviation from the Bragg condition. We will underline the analogy with Fraunhofer diffraction as known for classical optics.

2. Ideal monochromatic point source

We consider first the case where the incident beam is a spherical wave emitted by an ideal point source (an electron oscillating at a given frequency), located at a finite distance from the crystal. Using the current terminology in X-ray dynamical theory, 'spherical wave' means a point source located on the entrance surface, a case analyzed in detail by Kato. This holds for a conventional laboratory source, where the source is so near to the sample that a stationary-phase approximation is well justified (Authier & Simon, 1968). This simplification is not valid for the present generation of synchrotron sources. However, the incident wave cannot be considered as a plane wave either. A criterion commonly used in optics (Born & Wolf, 1983, Section 9.3) in considering the incident wave as plane is that the distance between the spherical wave front and its tangential plane be smaller than $\lambda_0/2$:

$$L_0(\Delta\theta)^2 \ll \lambda_0/2, \qquad (1)$$

where λ_0 is the wavelength of incident wave, L_0 is the source-to-crystal distance and $\Delta\theta$ is the angular divergence of the source as seen by the illuminated region of the crystal (see Fig. 1). The source divergence $\Delta\theta$ is limited to the effective angular acceptance of the crystal, known as the Darwin width.

Consider, as an example, an incident beam with a divergence $\Delta\theta \sim 10^{-5}$, *i.e.* the illuminated region on the crystal is 1.45 mm wide at a distance $L_0 = 145$ m, which is the source distance at the ID19 beamline at ESRF (European Synchrotron Radiation Facility), and $\lambda_0 \sim 10^{-10}$ m: the condition (1) is far from being satisfied.

It is convenient to express the incident spherical wave

$$\psi_0^{\rm inc}(\mathbf{r}, k_0) = A \exp(-2\pi i k_0 r) \quad (2)$$

in the form of a modulated plane wave:

$$\psi_0^{\rm inc}(\mathbf{r}, k_0) = D_0^{\rm inc}(\mathbf{r}) \exp(-2\pi i \mathbf{k}_0 \cdot \mathbf{r}), \quad (3)$$

where we do not explicitly specify the amplitude term A, which is not relevant in our analysis.

Let us call O the origin of the ξ axis, where the Bragg condition is satisfied exactly for λ_0 (Fig. 2), $\mathbf{r}$ is equal to $\overline{SP}$ and the vector $\mathbf{k}_0$ is along $\overline{SO}$. The amplitude $D_0^{\rm inc}$ of the incident wave (3) on the entrance surface can be written in paraxial approximation ($\Delta\theta = \xi \cos\theta_B / L_0 \ll 1$):

$$D_0^{\rm inc}(\xi) = \exp[i\pi(\cos^2\theta_B/\lambda_0 L_0)\xi^2], \quad (4)$$

where θ_B is the Bragg angle.

Similarly, the diffracted amplitude on the exit surface is expressed as

$$\psi_h(x) = \exp[-2i\pi(\sin\theta_B/\lambda_0)x] D_h(x), \quad (5)$$

where O' is the origin of the x axis (Fig. 2).

The diffracted pseudo-amplitude $D_h(x)$ on the exit surface can be obtained from the pseudo-amplitude on the entrance surface $D_0^{\rm inc}(\xi)$ [equation (4)] by means of a propagator $T(\xi)$ given in Takagi's generalized dynamical theory, in the case of a perfect crystal (Takagi, 1969; Authier & Simon, 1968):

$$\begin{aligned} D_h(x) &= \int_{x+l}^{x-l} D_0^{\rm inc}(\xi) T(x-\xi)\, {\rm d}\xi \\ &= \int_{-l}^{+l} \exp[i\pi(\cos^2\theta_B/\lambda_0 L_0)(x-\xi_1)^2] T(\xi_1)\, {\rm d}\xi_1 \end{aligned} \quad (6)$$

using (4) with $\xi_1 = x - \xi$.

T is the Green function or propagator, which can be obtained by means of the Riemann method from the Takagi–Taupin equations in the case of a perfect crystal (Takagi, 1969); it can also be obtained in a straightforward way (Guigay, 1999).

For a symmetrical reflection, this function has nonzero values in the interval $|\xi| < l$, with $l = t\tan\theta_B$, where t is the crystal thickness:

$$T(\xi) = \begin{cases} i\pi(k_0\chi_h/2\sin\theta_B)\exp[-\pi i \chi_0 k_0 (t/\cos\theta_B)] \\ \quad \times J_0[2\pi k_0(\chi_h\chi_{-h})^{1/2}(l^2-\xi^2)^{1/2}] & |\xi| < l \\ 0 & \text{elsewhere} \end{cases} \quad (7)$$

where J_0 is the zero-order Bessel function, $k_0 = 1/\lambda_0$ and χ_0, χ_h, χ_{-h} are the Fourier components of the susceptibility.

3. Locally plane wave

3.1. The locally plane wave approximation

The case of a spherical wave emitted by a source located at a distance of the order of a few tens of centimetres was considered years ago by Authier & Simon (1968). They showed that the exponential term in the formula (6) oscillates so rapidly that the integral can be evaluated by the stationary-phase method. In this case, $D_h(x)$ is equal to $T(x)$ [equation (7)], which is the 'spherical-wave' solution given by Kato (1961*b*). Afanas'ev & Kohn (1977) have studied the case of a source located at a finite distance in a more general way and experiments have been performed by Aristov *et al.* (1980). They have observed *Pendellösung* fringes oriented in a sense opposite to Kato's fringes.

Synchrotron sources are very far from the crystal and the quadratic term in the argument of the exponential varies slowly. The stationary-phase approximation is no longer applicable and conversely it is possible to use another approximation that turns out to be similar to the Fraunhofer approximation in classical optics.

We can write (6) in the form

$$D_h(x) = \int_{-l}^{+l} \exp[(i\pi\cos^2\theta_B/\lambda_0 L_0)(x^2 + \xi_1^2 - 2x\xi_1)] T(\xi_1)\, {\rm d}\xi_1. \quad (8)$$

The ξ_1^2 term can be neglected in (8) if

$$(\cos^2\theta_B/\lambda_0 L_0) l^2 \ll 1 \Rightarrow l \ll (1/\cos\theta_B)(\lambda_0 L_0)^{1/2} \quad (9)$$

because the integration is limited to the interval $[-l, l]$, which is the basis of the Borrmann triangle $P'MN$ (Fig. 2).

Since $l = t\tan\theta_B$, (9) can be expressed as

$$t \ll (1/\sin\theta_B)(\lambda_0 L_0)^{1/2} \equiv t_{lp}. \quad (10)$$

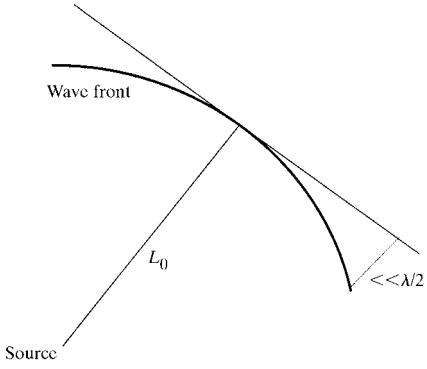

Figure 1
A spherical wave front can be approximated by its tangent plane in the region where the distance is $\ll \lambda/2$.

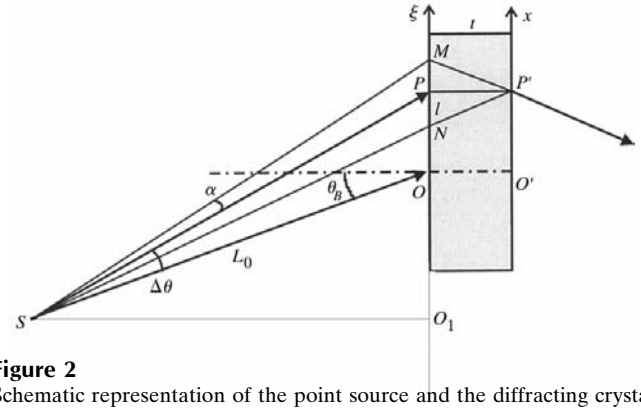

Figure 2
Schematic representation of the point source and the diffracting crystal.

Owing to the large source-to-sample distance L_0, it is possible to satisfy condition (10) for a rather large crystal thickness t of many hundreds of micrometres, much larger than the *Pendellösung* length Λ_0 (tens of micrometres). Usual samples fulfil both (10) and $t > \Lambda_0$. This ensures that the crystal is not 'thin' and that dynamical effects are important.

If the term ξ_1^2 is neglected, (8) becomes

$$\begin{aligned} D_h(x) &\simeq \exp[(i\pi \cos^2\theta_B/\lambda_0 L_0)x^2] \\ &\quad \times \int_{-l}^{+l} \exp[(2\pi i \cos^2\theta_B/\lambda_0 L_0)x\xi_1]T(\xi_1)\,\mathrm{d}\xi_1 \\ &= \exp[(i\pi \cos^2\theta_B/\lambda_0 L_0)x^2]\widetilde{T}[(x/\lambda_0 L_0)\cos^2\theta_B], \end{aligned} \quad (11)$$

where the limits of the integral can be extended to $[-\infty, +\infty]$ since the propagator T is zero outside $[-l, l]$. The symbol $\widetilde{\ }$ indicates the Fourier transform. $(x/\lambda_0 L_0)\cos^2\theta_B$ is the 'frequency' variable for this transform.

The intensity on the exit surface is the square modulus of the Fourier transform of the propagator T [equation (11)]:

$$I_h(x) = |\widetilde{T}[(\cos^2\theta_B/\lambda_0 L_0)x]|^2, \quad (12)$$

which represents (Authier & Simon, 1968) the reflectivity curve

$$R(\Delta\theta) = |\widetilde{T}[(\cos\theta_B/\lambda_0)\Delta\theta]|^2$$

of the crystal, also known as the rocking curve:

$$I_h(x) = R[(x/L_0)\cos\theta_B]. \quad (13)$$

In the plane-wave dynamical theory, the reflectivity curve is the angular intensity response of the crystal as a function of the departure from Bragg angle for an incident plane wave.

Equation (8) shows that point P', located on the exit surface, is influenced by the limited domain given by the Borrmann triangle, MNP', of basis $2l$ (see Fig. 2). It is not influenced by the incident wave outside MN. This was pointed out by Carvalho & Epelboin (1990), who have introduced the effective divergence α:

$$\alpha = l\cos\theta_B/L_0, \quad (14)$$

which is the useful angular aperture of the incident beam for any point P' of the exit surface.

Generally, condition (1) is not fulfilled for the global divergence $\Delta\theta$ but it may be satisfied for the effective divergence α. Physically, this means that along a segment of length l the incident wave may be considered as a plane wave. Thus, each point x of the exit surface sees a wave that is locally plane, with a deviation from the Bragg position given by $\Delta\theta = (x/L_0)\cos\theta_B$.

Thus, when condition (10) is verified, we may consider the incident wave as a *locally plane wave* for the diffraction process. In such a case, the intensity profile along the exit surface reproduces the angular Bragg reflection profile (rocking curve) of the crystal.

3.2. Numerical analysis of the locally plane approximation

The locally plane wave result (11), and consequently the validity of condition (10), can be numerically checked by

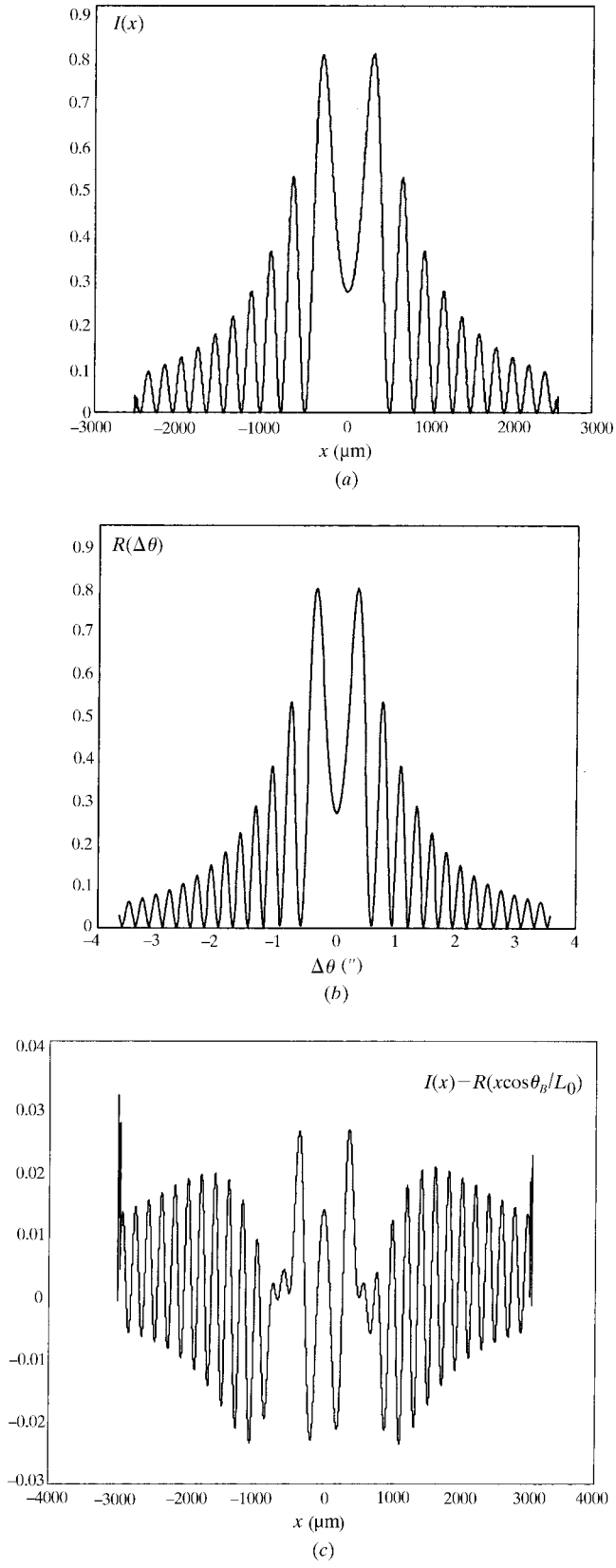

Figure 3
Computed intensity profile on the exit surface (*a*) and corresponding rocking curve (*b*), Si 111 reflection, thickness 300 μm, energy 30 keV. (*c*) Difference between (*a*) and (*b*) with the correspondence $\Delta\theta \rightleftharpoons x\cos\theta_B/L_0$.

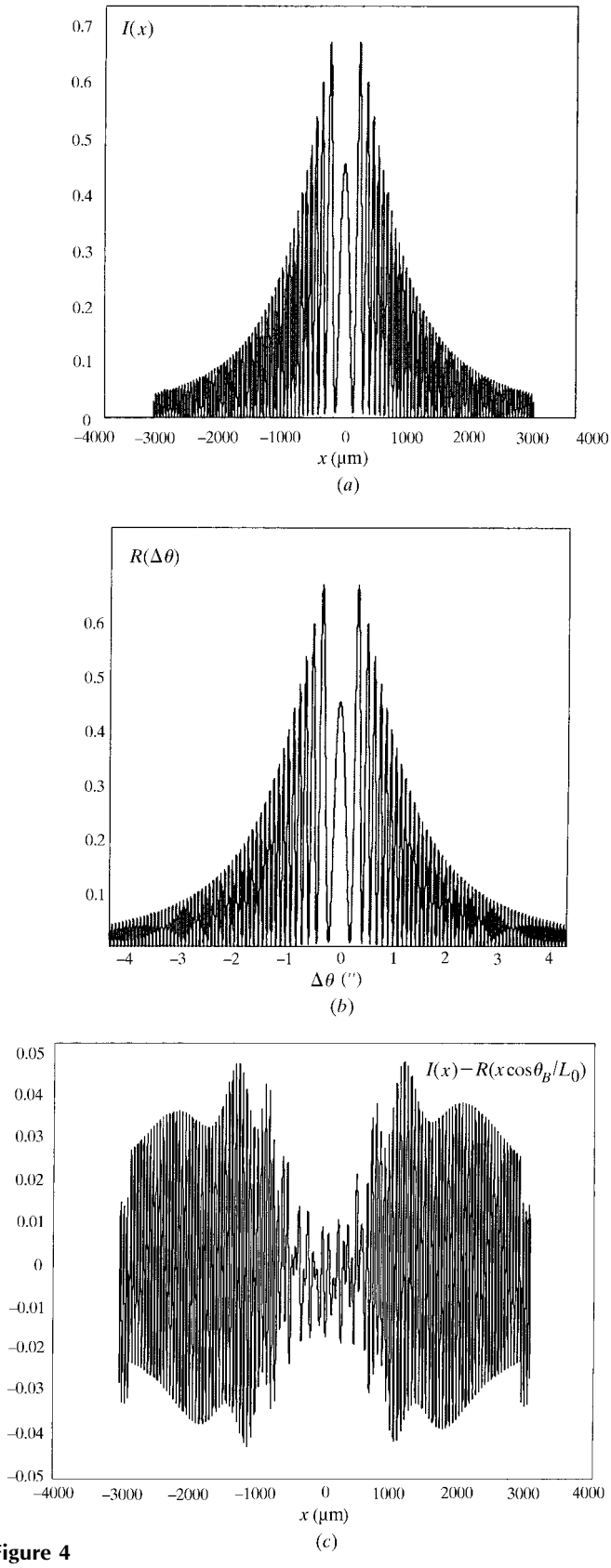

Figure 4
The calculated intensity profile on the exit surface (*a*) and the corresponding rocking curve (*b*), Si 111 reflection, 1200 μm thickness and an energy of 30 keV. (*c*) The difference between the two curves, with the correspondence $\Delta\theta \rightleftharpoons x\cos\theta_B/L_0$. The difference remains lower than a few percent.

integrating (6) directly and comparing the two results. We have analyzed the case of Si 111, at an energy of 30 keV. In this case, the critical-thickness value is $t_{lp} = 1188$ μm. Fig. 3(*a*) shows the intensity calculated for a thickness $t = 300$ μm, where condition (10) is well verified, together with the theoretical intrinsic profile $R(\Delta\theta)$ (Fig. 3*b*). Equation (13) is nicely verified, as shown in Fig. 3(*c*), which shows the difference between $I_h(x)$ and R_h, drawn as a function of the variable $(x/L_0)\cos\theta_B$.

The same calculation made for a crystal thickness $t = 1200$ μm, which is just above the limit t_{lp}, shows that the approximation is still valid within a few percent (Fig. 4*c*).

4. Partial coherence effects

4.1. Finite source size: spatial coherence

Up to now, we have considered an ideal point source. The finite size of a real source implies a finite coherence width of the incidence beam on the entrance surface of the crystal. Third-generation synchrotrons are characterized by two important features: the source is very small and the distance to the sample is very large, which gives a very high degree of spatial coherence. Measurements performed at ID19 at ESRF have shown that the coherence width is of the order of 100 μm (Cloetens *et al.*, 1997).

Taking into account the finite size of the source would mean introducing a mutual intensity function (Born & Wolf, 1983). However, we may simplify this problem because we are mainly interested in conditions for which the source size significantly changes the intensity profile along the exit surface, thus we will just compute the convolution of the intensity profile of the source with the intensity curve obtained for a point source.

The source can be described as a distribution of elementary incoherent quasi-monochromatic sources of infinitesimal size $d\xi$. This is discussed, in the case of synchrotron sources, by Coïsson (1995).

The beam coming from a point source shifted by ε (Fig. 5) meets the Bragg condition at a point on the entrance surface shifted exactly by ε with respect to the origin O. Let us call I_S

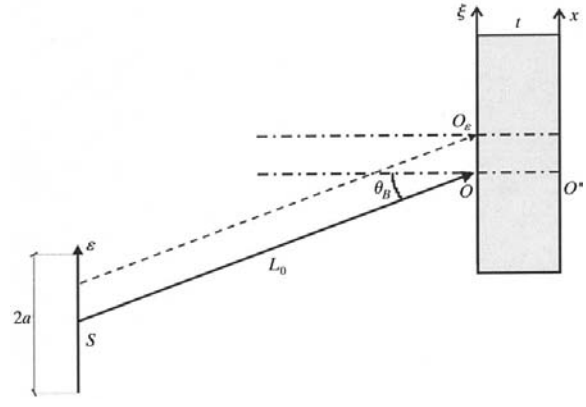

Figure 5
Effect of the source size: it can be interpreted as a shift of the point where the beam impinges at exact Bragg incidence.

the intensity distribution of the source. The intensity along the exit surface, previously given by (6), becomes

$$I_h(x) = \int I_S(\varepsilon)\,\mathrm{d}\varepsilon \int_{x+l}^{x-l} \exp[(i\pi\cos^2\theta_B/\lambda_0 L_0)(\xi_1-\varepsilon)^2] \times T(x-\xi_1)\,\mathrm{d}\xi_1 \int_{x+l}^{x-l} \exp[-(i\pi\cos^2\theta_B/\lambda_0 L_0)(\xi_2-\varepsilon)^2] \times T^*(x-\xi_2)\,\mathrm{d}\xi_2. \quad (15)$$

Developing the squares in the exponential arguments, inverting the integral order and noting that ε^2 terms cancel out, we get

$$I_h(x) = \int_{x+l}^{x-l} \mathrm{d}\xi_2 \int_{x+l}^{x-l} \exp[(i\pi\cos^2\theta_B/\lambda_0 L_0)(\xi_1^2-\xi_2^2)]T(x-\xi_1) \times T^*(x-\xi_2)\,\mathrm{d}\xi_1 \int I_S(\varepsilon)\exp[(2i\pi\cos^2\theta_B/\lambda_0 L_0) \times (\xi_1-\xi_2)\varepsilon]\,\mathrm{d}\varepsilon. \quad (16)$$

The last integral is the mutual intensity function of the incident beam on the entrance surface (Born & Wolf, 1983). It is equal to the Fourier transform of the intensity source profile $I_S(\varepsilon)$ using the 'frequency' variable $(\cos^2\theta_B/\lambda_0 L_0)(\xi_1-\xi_2)$.

Assuming a Gaussian source profile of half width a, the transform is a Gaussian of half width $1/a$ (the Gaussian assumption is used only for simplicity because all other profiles give substantially the same results).

We may consider the last integral to be constant for small values of $\xi_1-\xi_2$, namely if

$$\xi_1-\xi_2 < \lambda_0 L_0/a\cos^2\theta_B. \quad (17)$$

The difference $\xi_1-\xi_2$ has an upper bound of $2l$ because of the limited interval of the integration over ξ_1 and ξ_2 [equation (16)].

This implies that condition (17) can be written

$$2l < \lambda_0 L_0/a\cos^2\theta_B \quad (18)$$

or, equivalently, since $t = l/\tan\theta_B$:

$$t < \lambda_0 L_0/a\sin 2\theta_B \equiv t_{sc}. \quad (19)$$

$\lambda_0 L_0/a$ in (18) is the spatial (or transverse) coherence width at a distance L_0 from a quasi-monochromatic incoherent source of size a, as usually defined in optics for a quasi-monochromatic incoherent extended source [Van Cittert–Zernike theorem (Born & Wolf, 1983)].

4.2. Finite source bandwidth: temporal coherence

Let us now introduce the nonmonochromaticity of the beam. For a given diffraction vector, the significant bandwidth is of the order of the Darwin width. We assume that the transfer function T does not change significantly in such an interval $\Delta\lambda$. However, the position of the point where the beam impinges at exact Bragg angle (O for λ_0 in Fig. 6) changes as a function of the wavelength, because the Bragg angle is a function of λ.

This can be described using the previous formalism assuming an incident monochromatic spherical wave, of wavevector $k = k_0 + \Delta k$. The polychromaticity is included in the modulation of the pseudo-amplitude, similarly to the sphericity of the wave front. Thus, the incident wave is expressed in the same way as (4), where the pseudo-amplitude is now

$$D_0^{\mathrm{inc}}(\xi, \Delta k) = \exp[(i\pi/\lambda_0 L_0)\xi^2]\exp(2\pi i\sin\theta_B\xi\Delta k). \quad (20)$$

The analysis of temporal coherence can be performed similarly to that of the spatial coherence, leading to an integral analogous to (16):

$$I_h(x) = \int_{x+l}^{x-l}\int_{x+l}^{x-l} \exp[(i\pi\cos^2\theta_B/\lambda_0 L_0)(\xi_2^2-\xi_1^2)]T(x-\xi_1) \times T^*(x-\xi_2)\,\mathrm{d}\xi_1\,\mathrm{d}\xi_2 \int_{k_0-\Delta k}^{k_0+\Delta k} I_\lambda(\Delta k) \times \exp[-2\pi i\sin\theta_B(\xi_1-\xi_2)\Delta k]\,\mathrm{d}\Delta k. \quad (21)$$

In the case of a white incident beam, the last integral becomes a δ function. Then, for a white beam, the illumination on the entrance surface is completely incoherent, as explained by Carvalho & Epelboin (1990).

Let us consider now the general case of an incident beam with a finite bandwidth $[-\Delta k_M, \Delta k_M]$. By analogy with the

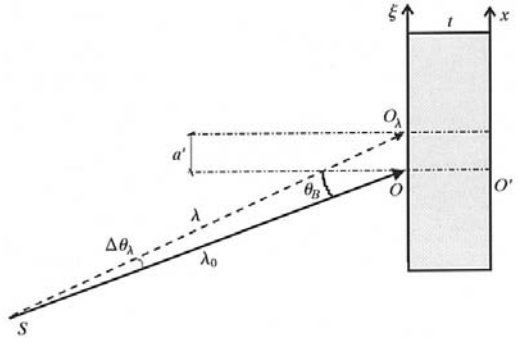

Figure 6
Effect of the polychromaticity: it can be interpreted in terms of an equivalent source size a'.

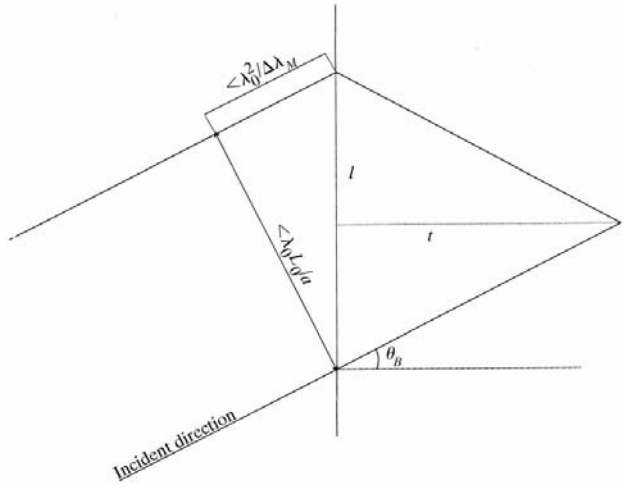

Figure 7
The coherence requirements can be interpreted in terms of the width and length of the wavepacket.

previous spatial coherence analysis, the integral over Δk can be considered as constant if

$$\sin\theta_B(\xi_1 - \xi_2) < (1/\Delta k_M) \Rightarrow (\xi_1 - \xi_2) < (1/\Delta k_M \sin\theta_B). \quad (22)$$

Polychromaticity does not change the intensity profile if

$$2l < 1/\Delta k_M \sin\theta_B = \lambda_0^2/\Delta\lambda_M \sin\theta_B \quad (23)$$

or, when expressed as a function of the thickness t,

$$t < \lambda_0^2/(2\Delta\lambda_M \tan\theta_B \sin\theta_B) = \lambda_0 d/(\Delta\lambda_M \tan\theta_B) \equiv t_{lc}, \quad (24)$$

where d is the interplanar distance.

Condition (24), or (23), is independent of the source distance and contains the term $\lambda_0^2/\Delta\lambda$, which is the temporal coherence length, as defined in classical optics.

If the locally plane wave approximation is applicable, the strong analogy with the influence of the source size is evident. In fact, the pseudo-amplitude on the exit surface (20) is, for a given Δk:

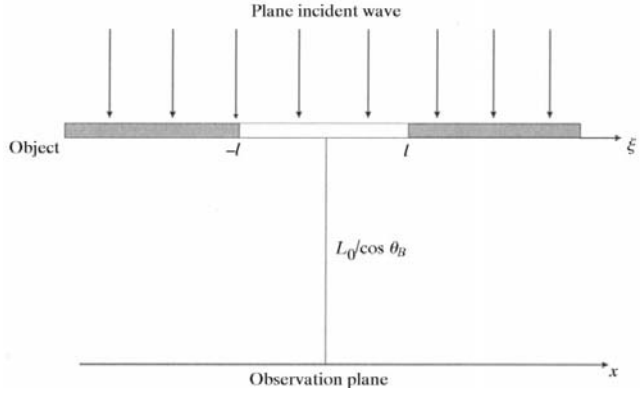

Figure 8
In classical optics, equation (6) represents the diffraction figure in a plane at a distance $L_0/\cos\theta_B$ of an object illuminated by a plane wave. The object is not merely a slit but has a transmission function $T(\xi)$.

$$D_h(x, \Delta k) = \exp\left(\frac{i\pi\cos^2\theta_B}{\lambda_0 L_0}x^2\right)\tilde{T}\left(\frac{\cos^2\theta_B}{\lambda_0 L_0}x - \sin\theta_B\Delta k\right), \quad (25)$$

where the phase term in (20) results in a translation in the Fourier transform (25).

The same result as (24) can be obtained (Mocella *et al.*, 1999) by using the differential expression of the Bragg law and considering a 'virtual' source size a', given by

$$a' = L_0\Delta\theta_\lambda = L_0(\Delta\lambda/\lambda_0)\tan\theta_B. \quad (26)$$

To summarize, we may now say that, when conditions (19) and (24) are fulfilled, the incident wave can be considered as perfectly coherent for diffraction processes in a perfect crystal. In this case, we can consider the incident wave as perfectly monochromatic and emitted by a point source (4).

5. Locally plane wave: coherence requirements and *Pendellösung* fringes

The coherence requirements (19) and (24) can be 'physically' understood considering the case of a locally plane wave, as analyzed in §3. The intensity profile (12) shows oscillations that are the well known plane-wave *Pendellösung* fringes. They arise from the interference of two wavefields inside the crystal, as described by the dynamical theory (see *e.g.* Ewald, 1917; Laue, 1931; Batterman & Cole, 1964; Pinsker, 1978). It is obvious that the interfering beams must be coherent. As pointed out in previous sections, a point on the exit surface is influenced by the incident wave only along the basis of the Borrmann fan. Condition (18) means that the lateral (spatial) coherence of the incident beam, $\lambda_0 L_0/a$, has to be larger than the basis of the Borrmann fan projected orthogonally on the incidence direction ($2l\cos\theta_B$):

$$(\lambda_0 L_0/a) > 2l\cos\theta_B. \quad (27)$$

The corresponding condition for the temporal (or longitudinal) coherence width of the incident beam (24) means that

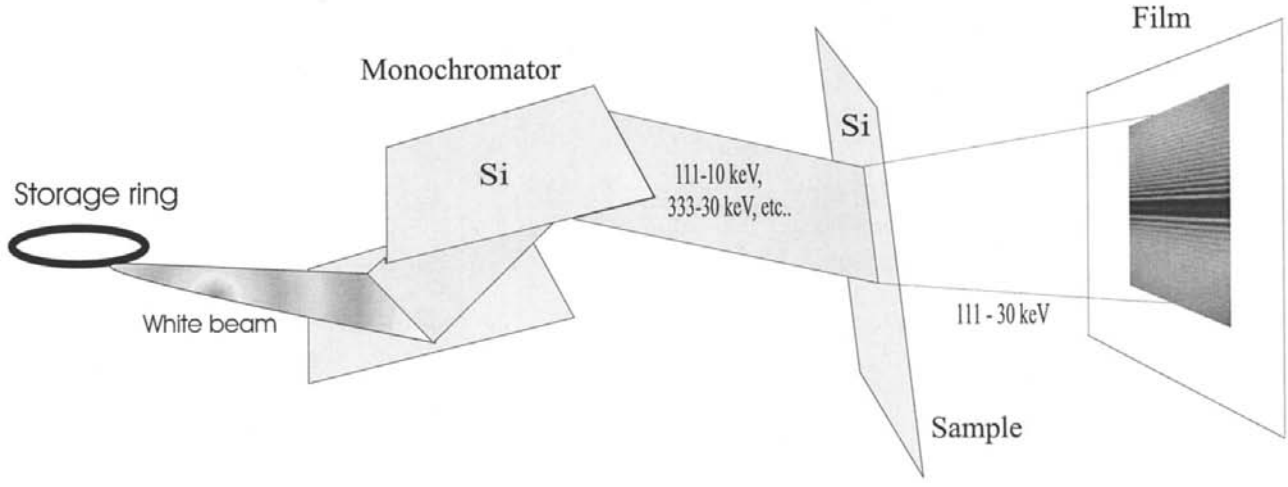

Figure 9
Experimental set-up.

$\lambda_0^2/\Delta\lambda$ has to be larger than the basis of the Borrmann fan projected along the direction of propagation ($2l\sin\theta_B$):

$$\lambda_0^2/\Delta\lambda > 2l\sin\theta_B. \quad (28)$$

We can summarize by saying that conditions (27) and (28) represent the width and the length of the incident wave packet. If these conditions are not fulfilled, interferences are not possible and the *Pendellösung* fringes disappear (Fig. 7).

As for classical optics, it is also possible to look at the coherence conditions in terms of simple fringes blurring. Outside the area close to its center, the intensity profile (13) is made of regularly spaced fringes, with a fringe spacing F_{sp} given by the expression for R (Pinsker, 1978):

$$F_{sp} = \lambda L_0/t\sin(2\theta_B). \quad (29)$$

To be able to see the fringes, the source size and the finite bandwidth of the source must be small enough. An elementary source located at point O_ε of coordinate ε (Fig. 5) produces an intensity profile, on the exit surface, displaced by ε. The different sources are incoherent with each other, thus the intensity profile is made of the superposition of all profiles produced by the different elementary sources. To be able to distinguish the fringe structure, the maximum displacement, *i.e.* the source size a, must be smaller than the fringe spacing (29):

$$a < \lambda L_0/t\sin(2\theta_B). \quad (30)$$

This condition is identical to (19).

Similarly, the finite bandwidth $\Delta\lambda$ of the incident beam induces a displacement of the point at exact Bragg position (Fig. 6) and can be linked to a virtual source of finite size a' [equation (26)], expressing the same condition as (24).

6. Locally plane wave and Fraunhofer approximation

It should be noticed that (6) has the form of a convolution integral that describes Fresnel diffraction in classical optics (Born & Wolf, 1983). In this case, $T(x)$ would be the transmission function of a transparent object of limited lateral size $\ell = 2l$ illuminated by a plane monochromatic wave of wavelength λ; $D_h(x)$ would be the wave amplitude in an observation plane at distance $L = L_0/\cos\theta_B$ (Fig. 8).

The Fresnel diffraction phenomenon contains two limiting cases:

(i) If $L \gg \ell^2/\lambda$, one speaks of *Fraunhofer diffraction*. The convolution integral is then reduced to the Fourier transform of the transmission function of the object $T(x)$.

(ii) If $L \rightarrow 0$, it can be shown that the convolution kernel $\exp[i\pi(x-\xi)^2/\lambda_0 L]$ tends to a δ distribution $\delta(x-\xi)$, with the obvious meaning that the diffraction pattern is then identical to the transmission function of the object $T(x)$.

Returning to our problem of X-ray diffraction, we underline that the locally plane approximation corresponds to the limiting case (1) of classical optics, namely to Fraunhofer diffraction.

Condition (9) can be rewritten as a Fraunhofer diffraction condition:

$$L > l^2/\lambda.$$

Similarly, Kato's spherical wave corresponds to the limiting case (ii) of classical optics.

The discussion by Afanas'ev & Kohn (1977) can be understood as the analysis of the transition between these two limiting cases.

7. Experimental results

Experiments have been performed at the ID19 beamline at the ESRF (source-to-sample distance $L_0 = 145$ m) to verify the above theoretical conclusions. To satisfy the good monochromaticity requirement, the incident beam was monochromated using the 333 reflection of the silicon nondispersive double-crystal monochromator installed on the line. The monochromator is set for (111) reflection at 10 keV and the sample itself was a silicon crystal oriented for (111) reflection

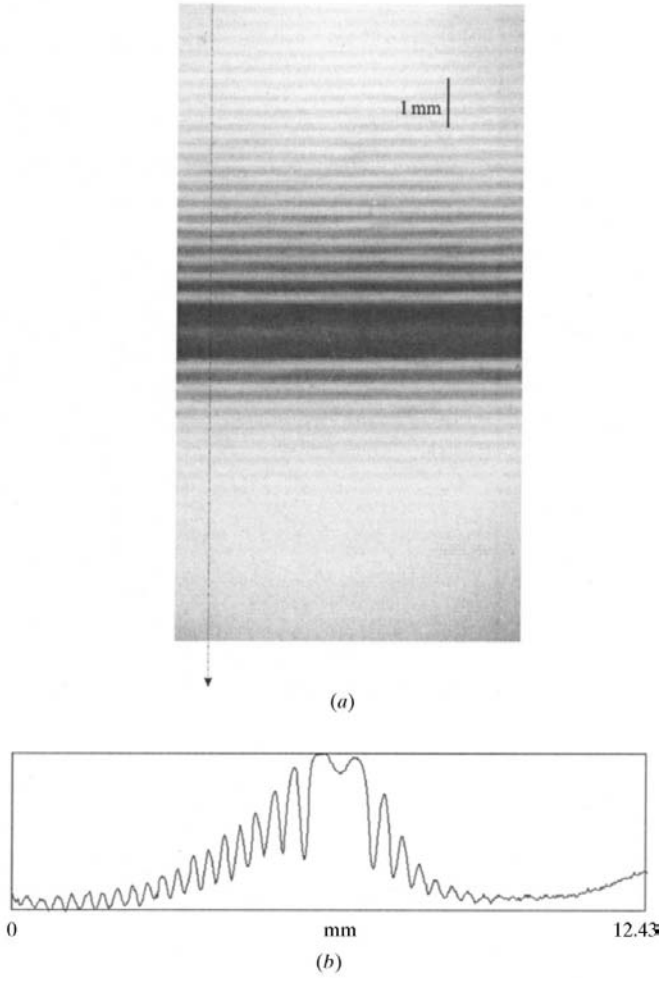

Figure 10
Photographic image for a silicon crystal thickness of 150 µm (111 reflection and 30 keV energy) under the locally plane wave condition. The recorded intensity reproduces the well known profile of the rocking curve (*b*), even if the nonlinearity of the photographic film used does not permit a precise comparison.

at 30 keV ($\lambda = 3.764$ Å, $\theta_B = 3.44^\circ$), corresponding to the third harmonic of the monochromator (Fig. 9). We chose a vertical setting because the smallest size of the source is in the vertical direction and is estimated approximately as $a = 50$ µm.

In this condition we get, according to (10), (19) and (24):

$$t_{lp} = 1188\ \mu\text{m}, \quad (31a)$$

$$t_{sc} = 912\ \mu\text{m}, \quad (31b)$$

$$t_{tc} = 433\ \mu\text{m}. \quad (31c)$$

We have choosen a sample of 150 µm thickness, which satisfies all the requirements $t < t_{lp}, t_{sc}, t_{tc}$. The observed image (Fig. 10) shows immediately that the recorded profile reproduces that of the rocking curve. Actually, the film saturation does not permit a precise comparison in intensity.

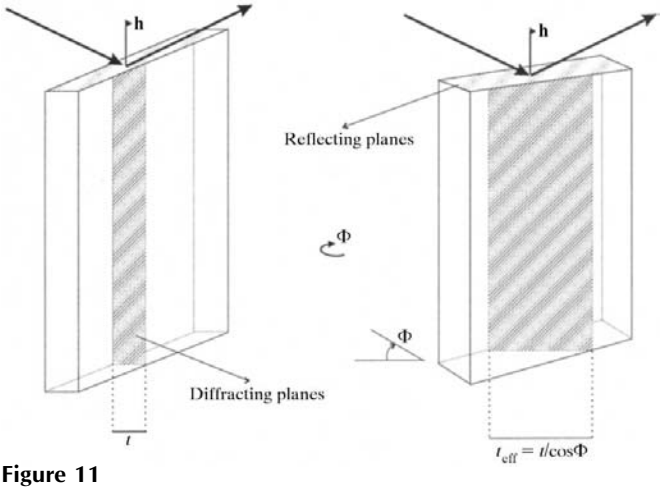

Figure 11
Rotating the crystal around the diffraction axis **h** changes the crystal thickness *seen* by the incident beam by a factor $1/\cos\Phi$.

The measured fringe separation, far from the center, where it becomes regular, is 305 µm, which is in very good agreement with the calculated value (29), $F_{sp} = 307$ µm. The small discrepancy may arise from the inaccuracy of the sample-thickness measurement: our method gives a more accurate thickness value.

In order to observe the changes in the profile with increasing thicknesses, we rotate the sample around the diffraction axis $\mathbf{h} \equiv (111)$ by an angle Φ. Thus, the effective thickness $t_{\rm eff}$ of the sample increases as $1/\cos\Phi$: $t_{\rm eff} = t/\cos\Phi$ (Fig. 11).

For a larger thickness, the fringe separation becomes smaller and conversely conditions (10), (19) and (24), especially the last one related to the temporal coherence, become more critical.

Fig. 12 shows the images taken for various rotation angles. For $\Phi = 60^\circ$, $t_{\rm eff} = 300$ µm is double the original one; the fringe separation is now about 150 µm. Condition (31*c*) is no longer fulfilled. The visibility of the fringes decreases owing to the lack of coherence. The fringe visibility could be used as an estimation of the coherence properties of the source, similar to the techniques that make use of ultra-plane waves (Ishikawa, 1988).

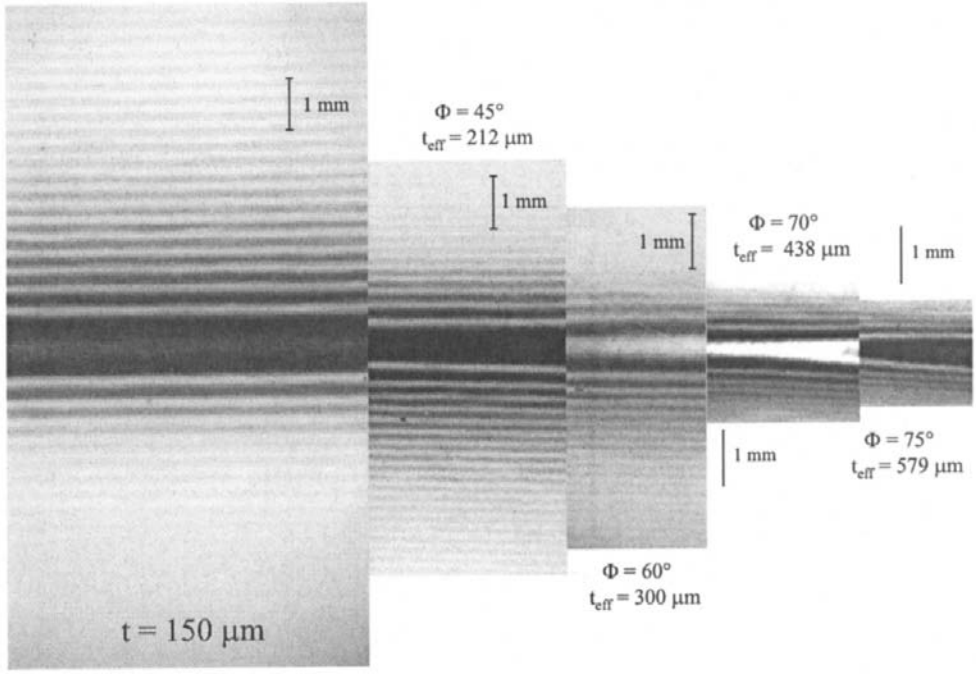

Figure 12
Images taken for various rotation angles Φ, corresponding to various effective thicknesses $t_{\rm eff}$. Rocking-curve oscillations are narrower for increasing thicknesses. When the coherence condition is no longer fulfilled ($\Phi = 70, 75^\circ$), the visibility of the fringes decreases.

8. Conclusions

We have shown that the sphericity of the wave front of the incident beam must be taken into account also for third-generation synchrotron sources. The incident wave cannot be considered as a truly plane wave. However, in some cases, the incident wave can be considered as 'locally plane'. In such cases, one can establish a local correspondence between the position along the surface and the angular deviation from the exact Bragg condition. The diffracted intensity on the film reproduces the angular rocking-curve profile of the crystal. The approximation of the locally plane wave allows interpretation of the coherence requirements for the incident beam. The coherence width and the coherence length of the incident wave packet must be larger than the width of the basis of the Borrmann triangle, in order to observe *Pendellösung* interference fringes along the exit surface.

The locally plane wave condition is equivalent to the Fraunhofer regime in classical optics.

We have shown experimental evidence of the locally plane wave phenomenon. Since the fringes are very sensitive to any deformation in the crystal or any change in the phase profile of the incident wave, this experiment can be used for high-precision diffraction studies. We will show in another paper how it can be used to study local deformation in crystals or phase objects which can be introduced in part of the incoming beam.

The authors wish to thank J. Härtwig and J. Baruchel for useful suggestions about the experimental set-up and their help in performing experiments. V. Mocella is indebted to the Istituto Nazionale per la Fisica della Materia (INFM) for his PhD fellowship.

References

Afanas'ev, A. M. & Kohn, V. G. (1977). *Sov. Phys. Solid State*, **19**, 1035–1040.
Aristov, V. V., Polovinkina, V. I., Afanas'ev, A. M. & Kohn, V. G. (1980). *Acta Cryst.* A**36**, 1002–1013.
Authier, A. & Simon, D. (1968). *Acta Cryst.* A**24**, 517–526.
Batterman, B. W. & Cole, H. (1964). *Rev. Mod. Phys.* **36**, 681–717.
Born, M. & Wolf, E. (1983). *Principle of Optics*, 6th ed. Oxford: Pergamon Press.
Carvalho, C. A. M. & Epelboin, Y. (1990). *Acta Cryst.* A**46**, 449–459.
Cloetens, P., Guigay, J. P., De Martino, C., Baruchel, J. & Shlenker, M. (1997). *Opt. Lett.* **22–14**, 1059–1061.
Coïsson, R. (1995). *Appl. Opt.* **34**, 904–908.
Ewald, P. P. (1917). *Ann. Phys. (Leipzig)*, **54**, 519–597.
Guigay, J. P. (1999). *Acta Cryst.* A**55**, 561–563.
Ishikawa, T. (1988). *Acta Cryst.* A**44**, 496–499.
Kato, N. (1960). *Acta Cryst.* **13**, 349–356.
Kato, N. (1961*a*). *Acta Cryst.* **14**, 526–532.
Kato, N. (1961*b*). *Acta Cryst.* **14**, 627–636.
Kato, N. & Lang, A. R. (1959). *Acta Cryst.* **12**, 787–794.
Laue, M. (1931). *Engeb. Exakt. Naturwiss.* **10**, 133–158.
Mocella, V., Guigay, J. P., Epelboin, Y., Härtwig, J., Baruchel, J. & Mazuelas, A. (1999). *J. Phys. D: Appl. Phys.* **32**, A88–A91.
Pinsker, Z. (1978). *Dynamical Scattering of X-rays in Crystals*. Berlin: Springer.
Takagi, S. (1969). *J. Phys. Soc. Jpn*, **26**, 1239–1253.